buildings

MDPI

Article

Intelligent Prediction and Application Research on Soft Rock Tunnel Deformation Based on the ICPO-LSTM Model

Chunpeng Zhang [1,2], Haiming Liu [1,2,*], Yongmei Peng [3], Wenyun Ding [1,4] and Jing Cao [1]

[1] Faculty of Civil Engineering and Mechanics, Kunming University of Science and Technology, Kunming 650500, China
[2] Key Laboratory of Earthquake Engineering and Engineering Vibration, Institute of Engineering Mechanics, China Earthquake Administration, Harbin 150080, China
[3] Faculty of Metallurgical and Energy Engineering, Kunming University of Science and Technology, Kunming 650093, China
[4] Kunming Survey, Design and Research Institute Co., Ltd. of CREEC, Kunming 650500, China
* Correspondence: haiming0871@163.com

Abstract: In tunnel construction, the prediction of the surrounding rock deformation is related to the construction safety and stability of the tunnel structure. In order to achieve an accurate prediction of the surrounding rock deformation in soft rock tunnel construction, a Long Short-Term Memory (LSTM) neural network is used to construct a prediction model of the vault settlement and the horizontal convergence of the upper conductor in soft rock tunnels. The crested porcupine optimisation (CPO) algorithm is used to realise the hyper-parameter optimisation of the LSTM model and to construct the framework of the calculation process of the CPO-LSTM model. Taking the soft rock section of the Baoshishan Tunnel as an example, the large deformation of the surrounding rock is measured and analysed in situ, and the monitoring data of arch settlement and superconducting level convergence are obtained, which are substituted into the CPO-LSTM model for calculation, and compared and analysed with traditional machine learning and optimisation algorithms. The results show that the CPO-LSTM model has an R^2 of 0.9982, a *MAPE* of 0.8595% and an *RMSE* of 0.1922, which are the best among all the models. In order to further improve the optimisation capability of the CPO, some improvements were made to the CPO and an Improved Crested Porcupine Optimiser (ICPO) was proposed. The ICPO-LSTM prediction model was established, and the ZK6 + 834 section was selected as a research object for comparison and analysis with the CPO-LSTM model. The results of the error analysis show that the prediction accuracy of the improved ICPO-LSTM model has been further improved, and the prediction accuracy of the model meets the requirements of guiding construction.

Keywords: improved crested porcupine optimise; soft rock tunnel; long short-term memory neural networks; intelligent prediction; deep learning

Citation: Zhang, C.; Liu, H.; Peng, Y.; Ding, W.; Cao, J. Intelligent Prediction and Application Research on Soft Rock Tunnel Deformation Based on the ICPO-LSTM Model. *Buildings* **2024**, *14*, 2244. https://doi.org/10.3390/buildings14072244

Academic Editor: Eugeniusz Koda

Received: 3 July 2024
Revised: 17 July 2024
Accepted: 19 July 2024
Published: 21 July 2024

1. Introduction

In recent years, with the continuous development of China's transportation construction, tunnel construction has the characteristics of long tunnel lines and a large excavation depth, which makes tunnel construction face more complex problems in the construction process. Tunnel soft rock deformation is one of the most prominent problems, especially in soft rock strata with poor rock mechanical properties, which are characterised by low rock strength and are prone to plastic deformation and damage. During tunnelling, deformation of soft rock can lead to settlement of the tunnel vault, increasing the risk of deformation and damage to surface and underground structures. It can also cause rock displacement, leading to the displacement and deformation of the tunnel wall, causing it to lose its load-bearing capacity and increasing the risk of tunnel collapse. It is therefore of great practical

engineering importance to carry out a working study on the prediction of deformation in soft rock tunnels.

With this problem in mind, a great deal of research has been carried out by scholars at home and abroad. In terms of numerical simulation, Yang Junsheng et al. [1] took the XHS tunnel of a high-speed railway through an arthritic coal shale layer as a basis, combined with on-site monitoring means and a discrete–continuous coupled numerical simulation to analyse the large deformation of the surrounding rock and damage characteristics, and based on the numerical simulation, proposed to take layers of pre-strengthening of the surrounding rock deformation control measures, and the results show that this method is an effective means of controlling the deformation of the surrounding rock in this type of arthritic coal shale layer. Guo Xinxin et al. [2] took the Muzailing road tunnel as a basis and used a combination of a three-dimensional computational model and multivariate linear regression to analyse the influence of the creep characteristics of the rock body on the deformation of the surrounding rock, and compared and analysed the predicted deformation and the actual deformation of the surrounding rock, and the results showed that the method has a certain degree of applicability. In terms of traditional prediction models, they mainly include the Grey Model [3,4], extreme learning machine [5,6] and support vector machine (SVM) [7]. However, the traditional prediction models have shortcomings in predicting tunnel rock deformation, such as a lack of ability to model nonlinear relationships, a lack of ability to learn complex patterns and sensitivity to noisy data. With the continuous development of the computational discipline, machine learning prediction methods play an increasingly important role in predicting the deformation of tunnel-surrounding rock. Due to its efficient fitting and generalisation ability, it has been successfully applied to tunnel rock deformation prediction [8–13].

Due to the extremely complex nature of the surrounding rock in mountain tunnels, there are many uncertainty factors with strong nonlinear characteristics. Traditional theoretical analysis and empirical analysis methods have difficulty in fully capturing this complex deformation mechanism, and the prediction results inevitably have some deviation. Although numerical simulation can simulate and analyse the deformation process of the surrounding rock, due to the relatively fixed parameter settings, it is difficult to fully reflect the dynamic changes of the actual state of the rock surrounding the tunnel. To overcome these problems, the attempt has been made to apply some new nonlinear prediction methods and machine learning techniques to the prediction of tunnel rock deformation. However, these methods still have some limitations when faced with long-time series data modelling and prediction, and it is difficult to fully exploit their potential [14,15]. In recent years, BP Neural Networks [16–18], Convolutional Neural Networks (CNNs) [19–21] and recurrent neural networks (RNNs) [22–24] have been widely applied to the analysis and prediction of deformation monitoring data. They have been found to have greater advantages than traditional prediction models when dealing with time series data. Yao et al. [25] established a generalised regression neural network tunnel deformation prediction model based on the Drosophila algorithm, and found that the Drosophila algorithm effectively improved the prediction accuracy of the model. Pan et al. [26] proposed an optimisation algorithm for predicting the dynamic nonlinear deformation of the surrounding rock, which improved the prediction accuracy of the dynamic neural network by optimizing the number of delay orders and the number of units of the hidden layer. Huang Zhen et al. [27] used a combined SVM-BP model, so that the combined model had a flexible nonlinear modelling capability and a parallel processing capability for large amounts of information. Xu et al. [28] used the numerical simulation method combined with an actual motorway tunnel project to determine its specific construction parameters, and predicted the deformation of the tunnel during the construction process using the LSTM algorithm, which provided guidance for the construction. Ye et al. [29] compared the prediction performance of four machine learning algorithms: a backpropagation neural network (BPNN), generalised regression neural network (GRNN), extreme learning machine (ELM), and particle swarm optimisation (PSO)- and genetic algorithm (GA)-optimised support vector machine. The

PSO-optimised GRNN model was found to have the smallest prediction error and the largest correlation coefficient. Kang et al. [30] further improved the prediction accuracy of the LSTM model by incorporating an attention mechanism into the model, which made the model more sensitive to parameters with higher weights. The Long Short-Term Memory (LSTM) neural network model has the advantages of fast convergence, high stability and high prediction accuracy when used to predict time series data [31].

The existing research results have laid a solid foundation for us to further promote the development of tunnel deformation prediction technology. Due to its excellent time-series modelling, nonlinear fitting, data fusion and feature learning capabilities, the LSTM model has obvious advantages in predicting the deformation of the rock surrounding a tunnel. Therefore, this paper proposes a long- and short-term memory neural network method based on the Crested Porcupine Optimiser to construct a deep learning prediction model for tunnel rock deformation, and investigates its effectiveness in predicting the deformation of the Jewel Mountain Tunnel of the Yunnan–Dabao Expressway. By comparing it with traditional optimisation algorithms and machine learning methods, this study verifies the accuracy and applicability of the CPO-LSTM model in the tunnel settlement time series prediction problem. In addition, this paper also makes some improvements to the CPO, constructs the ICPO-LSTM model and compares it with the CPO-LSTM model. This study shows that the optimisation ability of ICPO is further improved, the prediction progress of the ICPO-LSTM model is higher, and the accuracy and stability of the prediction are more consistent with the actual measurement data in the field. Using the ICPO-LSTM model to predict the deformation of soft rock tunnels not only promotes the practical application of artificial intelligence in tunnel construction, but also avoids construction risks in advance, reduces labour costs and improves the monitoring accuracy. It provides a new method for soft rock tunnel deformation monitoring.

2. Deep Learning Model of Long- and Short-Term Memory Neural Networks Based on Crested Porcupine Optimiser Algorithm

2.1. Basic Principles of the Crested Porcupine Optimiser

The Crested Porcupine Optimiser (CPO) is a new meta-heuristic algorithm proposed by Abdel-Basset et al. [32], and it has been studied to verify that the performance of the CPO is superior when compared to other traditional optimisation algorithms. The CPO simulates four defence strategies of the Crested Porcupine (CP), including sight, sound, odour and physical attack. The algorithm uses an exploratory and exploitative mechanism, where the first and second defence strategies (i.e., sight and sound) represent the exploratory behaviour of the CPO, while the third and fourth defence strategies (i.e., odour and physical attack) represent the exploitative behaviour of the CPO.

The first step is to initialise the population. Similar to other meta-heuristic population-based algorithms, the CPO starts the search process from the initial set of individuals (candidate solutions),

$$\vec{X}_i = \vec{L} + \vec{r} \times \left(\vec{U} - \vec{L}\right),\ i = 1, 2, \cdots, N' \tag{1}$$

where N' denotes the number of individuals (population size N'), $\vec{X}_i$ is the i-th candidate solution in the search space, $\vec{L}$ and $\vec{U}$ are the lower and upper bounds of the search range, respectively, and $\vec{r}$ is a random number between 0 and 1. The initial overall population can be expressed as

$$X = \begin{bmatrix} X_1 \\ X_1 \\ \vdots \\ X_i \\ \vdots \\ X_{N'} \end{bmatrix} = \begin{bmatrix} x_{1,1} & x_{1,2} & \cdots & x_{1,j} & \cdots & x_{1,d} \\ x_{2,1} & x_{2,1} & \cdots & x_{2,j} & \cdots & x_{2,d} \\ \vdots & \vdots & \vdots & \vdots & \vdots & \vdots \\ x_{i,1} & x_{i,2} & \cdots & x_{i,j} & \cdots & x_{i,d} \\ \vdots & \vdots & \vdots & \vdots & \vdots & \vdots \\ x_{N',1} & x_{N',2} & \cdots & x_{N',j} & \cdots & x_{N',d} \end{bmatrix} \tag{2}$$

Then, a cyclic population reduction technique (CPR) is used to obtain some CP from the population during the optimisation process, to speed up convergence and reintroduce them into the population to improve diversity and avoid falling into local minima. The cycle is based on a cyclic variable, to determine the number of times the process is executed during the optimisation process. The expression for the cyclic reduction of the population size is given below:

$$N = N_{min} + \left(N' - N_{min}\right) \times \left(1 - \left(\frac{t\%\frac{T_{max}}{T}}{\frac{T_{max}}{T}}\right)\right) \tag{3}$$

where T is the variable that determines the number of cycles, t is the current function evaluation, T_{max} is the maximum number of function evaluations, % denotes the remainder or modulus operator and N_{min} is the minimum number of individuals in the newly generated population, so that the size of the population cannot be smaller than N_{min}.

Finally, there are four separate defence strategies for entering the exploration phase.

(1) First defence strategy.

Its mathematical expression is shown below:

$$x = \vec{x} + \tau \times \left|2 \times \tau \times \vec{x} - \vec{y}\right| \tag{4}$$

where $\vec{x}_{CP}^{t}$ is the best solution of the evaluation function t, $\vec{y}_i^t$ is a vector generated between the current CP and a randomly selected CP from the population to represent the position of the predator at iteration t, τ_1 is a random number based on a normal distribution and τ_2 is a random value in the interval [0, 1].

The mathematical formula for generating is shown below:

$$\vec{y}_i^t = \frac{\vec{x}_i^t + \vec{x}_r^t}{2} \tag{5}$$

where r is a random number between [1, N].

(2) Second defence strategy.

Its mathematical expression is shown below:

$$\vec{x}_i^{t+1} = \left(1 - \vec{U}_1\right) \times \vec{x}_i^t + \vec{U}_1 \times \left(\vec{y} + \tau_3\left(\vec{x}_{r_1}^t - \vec{x}_{r_2}^t\right)\right) \tag{6}$$

where r_1 and r_2 are two random integers between [1, N] and are random numbers generated between 0 and 1.

(3) Third defence strategy.

Its mathematical expression is shown below:

$$\vec{x}_i^{t+1} = \left(1 - \vec{U}_1\right) \times \vec{x}_i^t + \vec{U}_1 \times \left(\vec{x}_{r_1}^t + S_i^t \times \left(\vec{x}_{r_2}^t - \vec{x}_{r_3}^t\right) - \tau_3 \times \vec{\delta} \times \gamma_t \times S_i^t\right) \tag{7}$$

where r_3 is a random number between [1, N], and $\vec{\delta}$ is a parameter used to control the direction of the search and is defined using Equation (8). $\vec{x_i^t}$ is the position of the i-th individual at iteration t, and γ_t is the defense factor defined using Equation (9). τ_3 is a random value in the interval [0, 1], and S_i^t is the odour diffusion factor defined using Equation (10), as shown below:

$$\vec{\delta} = \begin{cases} +1, & if \vec{rand} \leq 0.5 \\ -1, & Else \end{cases} \tag{8}$$

$$\gamma_t = 2 \times rand \times \left(1 - \frac{t}{t_{max}}\right)^{\frac{t}{t_{max}}} \tag{9}$$

$$S_i^t = exp\left(\frac{f(x_i^t)}{\sum_{k=1}^{N} f(x_i^k) + \varepsilon}\right) \tag{10}$$

where $f(x_i^t)$ denotes the value of the objective function for the i-th individual at iteration t, ε is a small value that avoids division by zero, $\vec{rand}$ is a vector that includes randomly generated values between 0 and 1, $rand$ is a variable that includes randomly generated numbers between 1 and 0, N is the overall size, t is the number of current iterations and t_{max} is the maximum number of iterations. The $\vec{U_1}$ vector is used to model the three possible scenarios in the strategy.

(1) When $\vec{U_1} = 0$, the CP will stop odour diffusion because the predator will stop moving because it is afraid of the CP, so the distance between the predator and the CP remains constant;
(2) When $\vec{U_1} = 1$, the CP will emit odour significantly because the predator is nearby;
(3) When $\vec{U_1}$ is within the interval range 0 and 1, the predator maintains a safe distance from the CP, at which time there is no need to emit its odour significantly.
(4) Fourth defence strategy.

Its mathematical expression is shown below:

$$\vec{x_i^{t+1}} = \vec{x_{CP}^t} + (\alpha(1 - \tau_4) + \tau_4) \times \left(\delta \times \vec{x_{CP}^t} - \vec{x_i^t}\right) - \tau_5 \times \delta \times \gamma_t \times \vec{F_i^t} \tag{11}$$

where $\vec{x_{CP}^t}$ is the best solution obtained, which denotes the position of the i-th individual of $\vec{x_i^t}$ at iteration t and denotes the predator at that position; α is the convergence speed factor discussed later in the parameter setting section; τ_4 is a random value in the interval [0, 1]; and $\vec{F_i^t}$ is the average force affecting the CP of the $i - th$ predator. It is provided by the inelastic collision law and defined by Equation (12),

$$\begin{gathered} \vec{F_i^t} = \vec{\tau_6} \times \frac{m_i \times \left(\vec{v_i^{t+1}} - \vec{v_i^t}\right)}{\Delta t} \\ m_i = \frac{f\left(\vec{x_i^t}\right)}{e\sum_{k=1}^{N} f\left(\vec{x_i^k}\right) + \varepsilon} \\ \vec{v_i^t} = \vec{x_i^t} \\ \vec{v_i^{t+1}} = \vec{x_r^t} \end{gathered} \tag{12}$$

where m_i is the mass of the $i-th$ individual (predator) at iteration t, $f(\cdot)$ denotes the objective function, $\vec{v}_i^{t+1}$ is the final velocity of the $i-th$ individual at the next iteration $t+1$ and is assigned based on the selection of a random solution from the current population, $\vec{v}_i^{t}$ is the initial velocity of the i-th individual at iteration t, Δt is the number of the current iteration and τ_6 is a vector including random values generated between 0 and 1.

In Equation (12), the average force of the CP is calculated based on dividing the numerator by the current iteration, and the average force of the current iteration increases linearly during the optimisation process, which causes the effect of the average force of the CP to diminish, and a small value of this factor is detrimental to the performance of the CPO. Therefore, by removing the numerator and relying only on the denominator, it is shown in Equation (13). This approach will help to create a wide range of values within the search space, resulting in a more comprehensive examination of the area around the solution.

$$\vec{F}_i^t = \vec{\tau}_6 \times m_i \times \left(\vec{v}_i^{t+1} - \vec{v}_i^{t}\right) \tag{13}$$

2.2. Basic Principles of the LSTM Model

The LSTM belongs to a temporal recurrent temporal network, which introduces a gating unit on the basis of a recurrent neural network, in order to memorise the historical state and control the information transfer, which overcomes the phenomena of gradient disappearance and gradient explosion. The memory unit module is located in the hidden layer, and for the basic structure, see Figure 1.

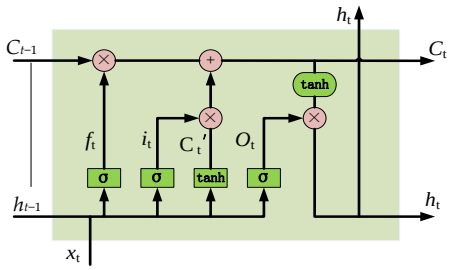

Figure 1. Unit structure of LSTM.

Each LSTM basic structure contains three types of gating structures, the forgetting gate f_t, the input gate i_t and the output gate O_t, which all use the sigmoid function (σ). The expression of the forgetting gate ft is as follows:

$$f_t = \sigma\left(x_t W_{xf} + h_{t-1} W_{h_{t-1}f} + b_f\right) \tag{14}$$

where W_{xf} is the weight matrix corresponding to the input x passed to f_t, $W_{h_{t-1}f}$ is the weight matrix corresponding to the state h_{t-1} passed to f_t at the previous time step and b_f denotes the bias term. The result of f_t is bounded between (0, 1) by the activation function σ.

The input gate is expressed as follows:

$$i_t = \sigma\left(x_t W_{xi} + h_{t-1} W_{h_{t-1}i} + b_i\right) \tag{15}$$

where W_{xi} is the weight matrix representing the input x_t passed to i_t, W is the weight matrix of the upper state h_{t-1} passed to i_t and b_i is the bias term. The computation of i_t is bounded between (0, 1) by the activation function σ.

The expression of the intermediate state C_t' is as follows:

$$C_t' = tanh\left(x_t W_{xC} + h_{t-1} W_{h_{t-1}C} + b_C\right) \tag{16}$$

where W_{xC} denotes the weight matrix corresponding to the input x_t passed to C'_t, $W_{h_{t-1}C}$ is the weight matrix corresponding to the upper state h_{t-1} passed to C'_t and b_C denotes the bias term. The computation result of C'_t is bounded between $(-1, 1)$ by the activation function *tanh*.

The expression of the output gate O_t is as follows:

$$O_t = \sigma\left(x_t W_{xO} + h_{t-1} W_{h_{t-1}O} + b_O\right) \tag{17}$$

where W_{xO} is the weight matrix that represents the input x_t transmitted to O_t, $W_{h_{t-1}O}$ is the weight matrix that represents the state h_{t-1} of the previous time step passed to O_t and b_O is the bias term. The computation result of O_t is bounded between (0, 1) by the activation function σ.

The output state h_t expression is as follows:

$$h_t = O_t \odot tanh(C_t) \tag{18}$$

That is, the output gate O_t is multiplied point-by-point with $tanh(C_t)$ to obtain the new output state at the current time step, which serves as part of the input for the next time step.

2.3. CPO-LSTM Model

The idea of constructing the CPO-LSTM model is to optimise the learning rate, hidden layer nodes and regularisation coefficients of the LSTM model by using the CPO optimisation algorithm. For a flowchart of the CPO-LSTM model, see Figure 2.

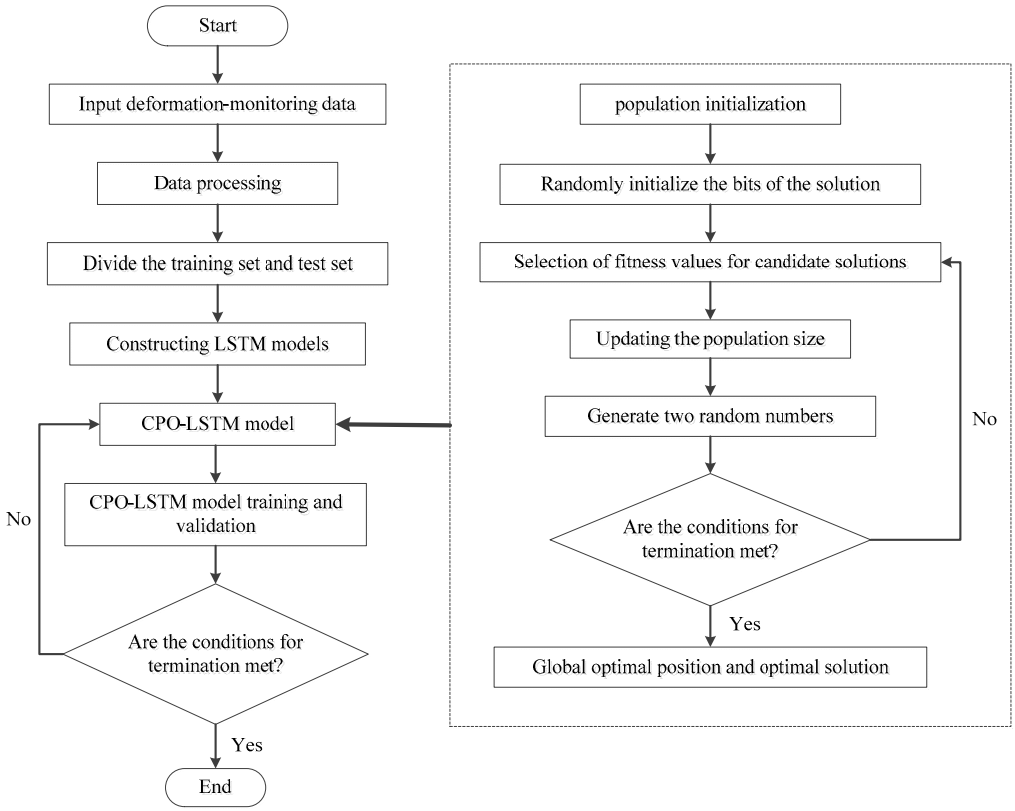

Figure 2. Flowchart of the CPO-LSTM model.

(1) Model initialisation.

The parameters of the CP are initialised, including the position of the crown porcupine, the upper and lower limits of the parameter values, and the maximum number of iterations.

Then, the LSTM structure is initialised, which uses the learning rate, the number of hidden nodes and the regularisation coefficient of the LSTM model as optimisation targets.

(2) Objective function establishment.

The objective function of the CP is the root mean square error (RMSE) of the predicted value of an untrained LSTM model compared to the actual value.

(3) Optimisation.

The position of the crowned porcupine is updated according to the result of the objective function, and the initial value of the LSTM is optimised when the initially set number of iterations is satisfied.

(4) LSTM training.

After optimizing the parameters, the optimal values are substituted into the LSTM model for re-training and prediction, ultimately yielding a predictive model.

2.4. CPO-GRNN Model

A generalised regression neural network (GRNN) is a four-layer forward propagation neural network with a good nonlinear approximation ability [33]; the data are input into the network and then pass through the input layer, pattern layer, summation layer and output layer in order to obtain the output result.

(1) Input layer: The input data is passed to the pattern layer, and the number of nodes is the feature dimension of the input data.

(2) Pattern layer: It generally uses a Gaussian function to process the input data, the number of nodes is the number of training samples, and the calculation formula is as follows:

$$g_i = exp\left(-\frac{\|x_i - x_j\|}{2\sigma^2}\right) \tag{19}$$

where x_i is the training sample, x_j is the learning sample and σ is the smoothing factor.

(3) Summation layer: Assuming that the output sample dimension is k, then the number of nodes in the layer is $k + 1$, where a node output S_D is the arithmetic sum of the output of the pattern layer, and the rest of the node outputs S_{Ni} are all weighted sums of the output of the pattern layer; the calculation formula is as follows:

$$S_D = \sum_{i=1}^{n} g_i \tag{20}$$

$$S_{Ni} = \sum_{i=1}^{n} w_{ij} g_i \tag{21}$$

where, w_{ij} is the weighting coefficient.

(4) Output layer: The number of nodes in this layer is the output sample dimension, which is mainly based on the arithmetic sum and weighted sum derived from the summation layer to calculate the output; the calculation formula is as follows:

$$O_j = \frac{S_{Ni}}{S_D} \tag{22}$$

For a flowchart of the CPO-GRNN model, see Figure 3.

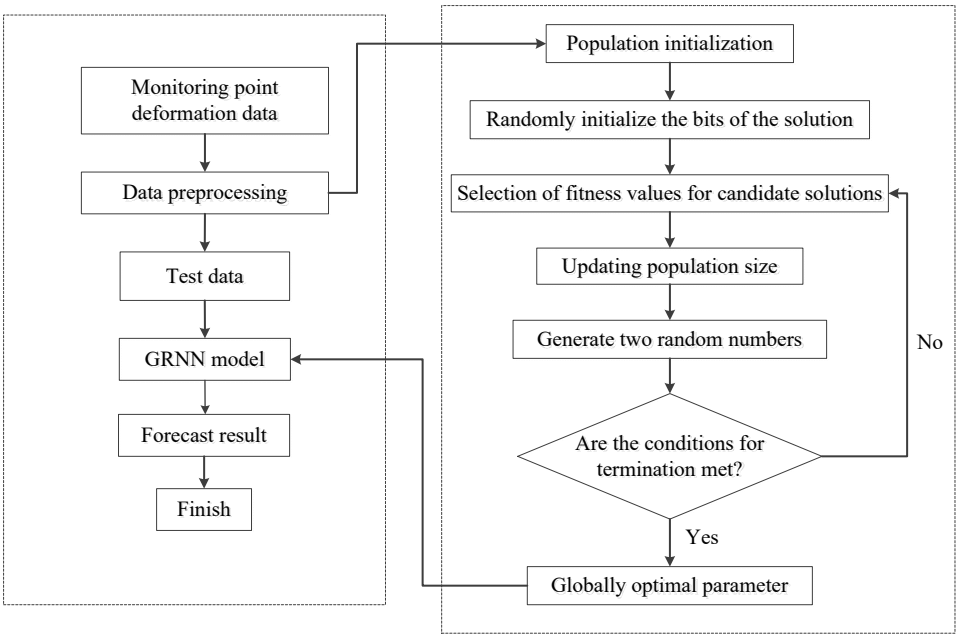

Figure 3. Flowchart of the CPO-GRNN model.

2.5. WOA-LSTM Model

The Whale Optimisation Algorithm (WOA) was first proposed by Mirjalili et al. [34] in 2016. The algorithm searches for the optimal solution by simulating the hunting behaviour of humpback whales—including three operators to simulate the hunting process of humpback whales' encircling predation, foaming net attack and prey search—from determining the search area to a local search, to the final implementation of a global search. The algorithm is characterised by a high accuracy and fast convergence, and has good performance in solving optimisation problems.

(1) Encircling predators: Humpback whales choose the optimal path to encircle their prey; the calculation formula is as follows:

$$D = \left|C \cdot X'(t) - X(t)\right| \tag{23}$$

$$X(t) = X'(t) - A \cdot D \tag{24}$$

where D is the distance between the prey and the optimal search agent; $X'(t)$ is the position of the prey; $X(t)$ is the position of the whale; t is the number of iterations; and A, C are coefficient vectors.

(2) Bubble net attack: The algorithm uses two ways to simulate humpback whale hunting behaviour. These two ways update the position of the humpback whale and then move it towards the prey according to the randomly generated probability of alternately updating the optimal search agent; the calculation formula is as follows:

$$X(t+1) = D'^{e^{bI}} cos 2\pi I + X'(t) \tag{25}$$

$$D' = \left|X'(t) - X(t)\right| \tag{26}$$

where b is the shape parameter of the logarithmic spiral and I is a random number between 0 and 1.

(3) Random search: There is a random search method among humpback whales, and the search phase can update the position according to the nearest search agent; the calculation formula is as follows:

$$D = |CX_{rand}(t) - X(t)| \tag{27}$$

$$X(t+1) = X_{rand}(t) - AD \tag{28}$$

where $X_{rand}(t)$ is the random position of the prey.

The WOA algorithm searches for the optimal process, generates a random number $q \in [0, 1]$ and enters the bubble net attack mode if $q > 0.5$; otherwise, the coefficient vector A is evaluated, and the target prey is searched for if $|A| \geq 1$ and encircled if $|A| \leq 1$. As the number of iterations of the WOA algorithm increases, it gradually transitions from the prey-seeking state to the prey-encircling state.

For a flowchart of the WOA-LSTM model, see Figure 4.

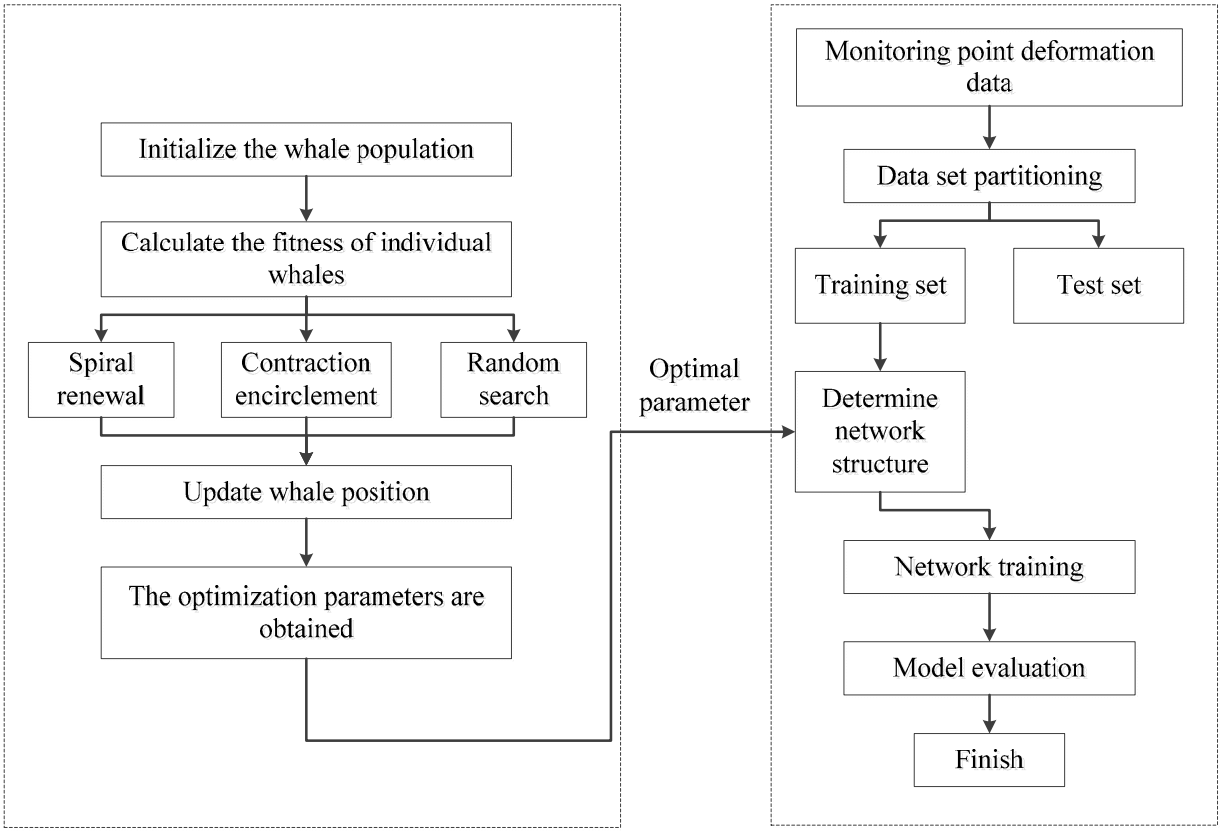

Figure 4. Flowchart of the WOA-LSTM model.

3. Numerical Modelling Experiments

3.1. Project Overview

The Baoshishan Tunnel is located in the north of Baoshan City, Yunnan Province. The left side of the tunnel start and stop pile numbers are ZK6 + 598~ZK10 + 134, the tunnel length is 3532.159 m, the maximum depth is 232.32 m; it belongs to the extra-long tunnels.

The project is located in the southern part of the Hengduan Mountains, located in the tail of the Nujiang Mountain Range and Gaolilongshan Mountain Range, set in the Lancang River and Nujiang River between regional terrain that is generally high in the north and low in the south. The highest point in the corridor of the project area is the peak of the southeast side of Qiushan Village, with a summit elevation of about 2256.72 m, and the ground elevation of Baoshan Damzi is about 1658 m, with a maximum elevation difference of 598.72 m. The geomorphology of the area is mainly controlled by tectonics, erosion, denudation, solvation and accretion. It belongs to the southwest Yunnan seismic zone, which is a seismic zone with very frequent strong seismic activities, with a high frequency

and intensity of seismic activities. Due to the long-term rise of the earth's crust, resulting in violent erosion of the water flow, the terrain cutting depth is greater.

3.2. Field Monitoring Data

In order to verify the accuracy and applicability of the model for predicting tunnel peripheral rock deformation, the monitoring and measurement data of section ZK6 + 834 at the tunnel mileage were selected as the research object, and the monitoring data of the vault settlement and the horizontal convergence of the upper conductor were collected at the site. For the layout of site monitoring points, see Figure 5. For the peripheral rock deformation monitoring data of the ZK6 + 834 section, see Table 1.

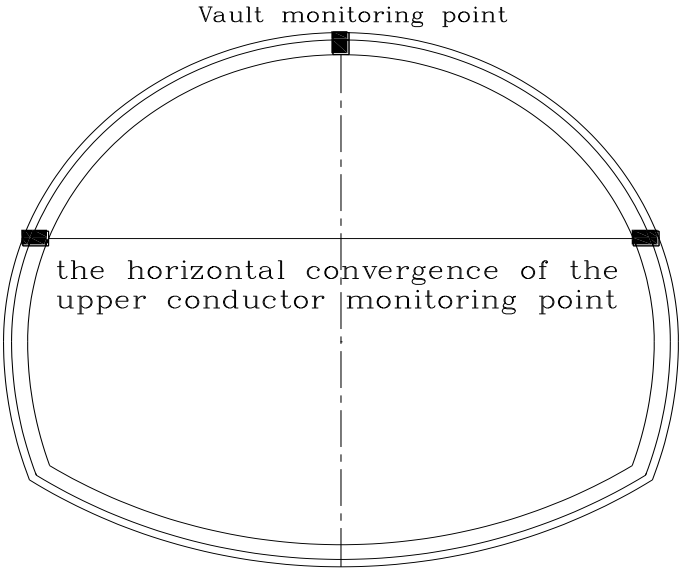

Figure 5. Field monitoring data points.

Table 1. Monitoring data of surrounding rock deformation of ZK6 + 834 section.

Time/d	Accumulated Deformation/mm		Time/d	Accumulated Deformation/mm		Time/d	Accumulated Deformation/mm	
	Vault	Upper Conductor		Vault	Upper Conductor		Vault	Upper Conductor
0	0	0	14	191.9	58.2	28	328.9	96.3
1	15.7	5.5	15	206.9	62.4	29	330.1	96.8
2	28.2	9.3	16	221.3	66.3	30	331.0	97.2
3	36.6	11.9	17	236.4	70.3	31	331.4	97.4
4	53.8	17.5	18	250.7	74.2	32	331.6	97.5
5	66.6	21.4	19	263.1	77.7	33	331.8	97.6
6	79.9	25.6	20	272.4	81.3	34	332.0	97.7
7	93	29.6	21	281.4	84.3	35	332.2	97.8
8	106	33.6	22	290.3	86.7	36	332.3	97.8
9	121.3	38	23	299.3	89.1	37	332.4	97.8
10	135.4	42.1	24	308.9	91.4	38	332.5	97.8
11	149.4	46.1	25	316.9	93.2	39	332.6	97.8
12	163.4	50.1	26	322.6	94.6			
13	177.6	54.1	27	327.2	95.7			

3.3. Numerical Test Verification

In this experiment, the CPO-LSTM, LSTM, CPO-GRNN and WOA-LSTM models are selected for comparison experiments, and the monitoring data in Table 1 are substituted into the models for computation; first, the model training set and test set are divided, the first 70% of the data set (27 groups) is used as the training set, and the second 30% of the

data set (12 groups) is used as the test set. The optimisation algorithm mainly optimises the learning rate, hidden layer nodes and L2 regularisation coefficients, and the activation function selects the nonlinear activation function ReLU. The learning rate and iteration number of the model are set to 0.02 and 50, respectively, and the optimisation algorithm globally searches for the optimal LSTM model hyper-parameters and completes the model construction. The prediction of the vault settlement and the horizontal convergence of the upper conductor is carried out, and the four models are iteratively trained; for comparison graphs of the vault settlement and the horizontal convergence of the upper conductor, see Figures 6 and 7, respectively.

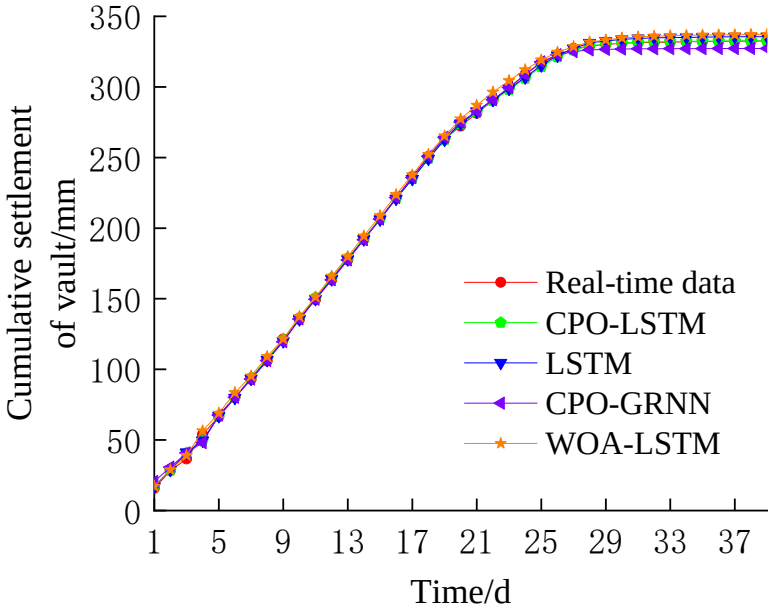

Figure 6. Comparative chart of cumulative settlement of arch crown between measured values and predicted values from different models.

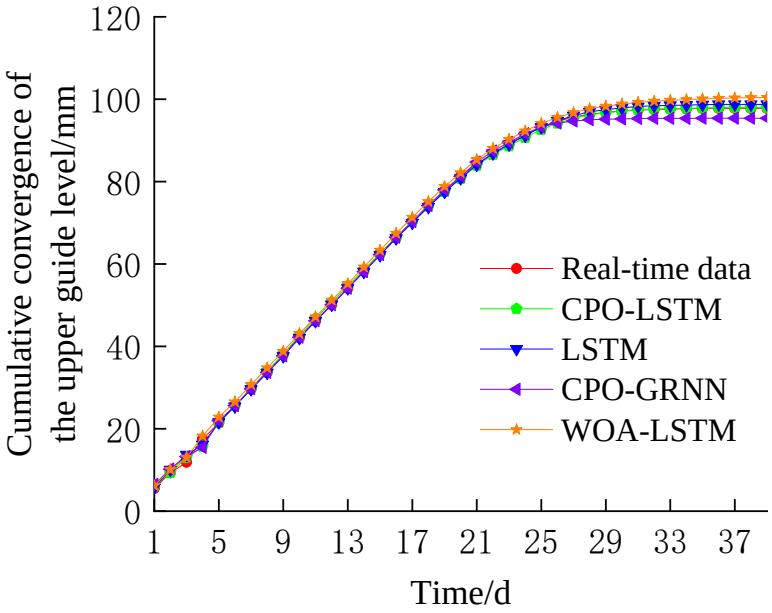

Figure 7. The comparative chart of the measured cumulative horizontal convergence of the upper guide and predicted values from different models.

From Figures 6 and 7, it can be seen that the CPO-LSTM model achieves an accurate prediction of the perimeter rock deformation in the ZK6 + 834 section, and the prediction

accuracy meets the requirements for construction guidance. Comparing the prediction curves of the CPO-LSTM and LSTM models, it can be seen that the LSTM model optimised by CPO has been improved in both fit and accuracy, which further improves the prediction accuracy of the LSTM model. Under the condition of different prediction models with the same optimisation algorithm, the CPO-LSTM model has a higher prediction accuracy than the CPO-RGNN model, which indicates that the LSTM deep learning method has a stronger advantage than the traditional machine learning method. Under the condition of different optimisation algorithms for the same prediction model, the CPO-LSTM model has higher fitting and prediction accuracies compared to the WOA-LSTM model, indicating that the optimisation ability of the CPO is stronger.

3.4. Model Performance Evaluation

In order to further evaluate the accuracy and generalisation of the model, three evaluation criteria, namely, the goodness of fit (R^2), mean absolute percentage error ($MAPE$), and root mean square error ($RMSE$), were used to assess the prediction accuracy of the prediction model, and the formulas are shown below:

$$R^2 = 1 - \frac{\sum_{k=1}^{n}(P_k - Q_k)^2}{\sum_{k=1}^{n}(P_k - \overline{Q})^2} \tag{29}$$

$$MAPE = \frac{1}{n}\sum_{k=1}^{n}\frac{|P_k - Q_k|}{Q_k} \times 100\% \tag{30}$$

$$RMSE = \sqrt{\frac{1}{n}\sum_{k=1}^{n}(P_k - Q_k)^2} \tag{31}$$

where n is the total number of samples, P_k is the predicted value of the kth sample and Q_k is the monitoring value of the $k-th$ sample and is the average of the monitoring values of all samples.

Substituting the experimental data of the CPO-LSTM, LSTM, CPO-GRNN and WOA-LSTM models into Equations (29) to (31), the evaluation indexes of each model can be obtained (see Table 2).

Table 2. Model performance evaluation form.

Predictive Modelling	Evaluation Indicators	ZK6 + 834 Section		Average Value
		Vault Monitoring Points	Upper Conductor Monitoring Point	
CPO-LSTM	R^2	0.9996	0.9998	0.9997
	$MAPE/\%$	0.6346	0.1107	0.3727
	$RMSE$	0.2262	0.1137	0.1700
LSTM	R^2	0.9991	0.9991	0.9991
	$MAPE/\%$	0.9012	0.8900	0.8956
	$RMSE$	2.9976	0.8740	1.9358
CPO-RGNN	R^2	0.9975	0.9929	0.9952
	$MAPE/\%$	1.4289	2.2858	1.8574
	$RMSE$	4.7731	2.2423	3.5077
WOA-LSTM	R^2	0.9984	0.9950	0.9967
	$MAPE/\%$	1.2797	2.2080	1.7439
	$RMSE$	4.2697	2.1867	3.2282

When the R^2 is larger and $MAPE$ and $RMSE$ are smaller, it indicates that the performance of the model is better. As can be seen from Table 2, the average value of R^2 of the evaluation results of the CPO-LSTM model is 0.9997, which is the largest among the four models, indicating that the CPO-LSTM model can respond well to the change rule of convergence of tunnel-surrounding rock deformation and can accurately predict the change trend of the surrounding rock. Meanwhile, the average values of $MAPE$ and $RMSE$ of the

CPO-LSTM model are the smallest among all the models, which are 0.3727% and 0.1700, respectively, indicating that the prediction accuracy of the CPO-LSTM model is the highest compared with the other models, and it is able to accurately predict the convergence of the tunnel-surrounding rock deformation and provide guidance for the actual project.

4. The Improved Crested Porcupine Optimiser (ICPO) Optimises the LSTM Model

4.1. Improved Crested Porcupine Optimiser (ICPO)

Through the validation of the numerical modelling experiments, it is concluded that the CPO-LSTM model has the best performance compared to the LSTM, CPO-GRNN and WOA-LSTM models. In order to further improve the optimisation ability of the CPO, some preliminary improvements are made.

(1) Remove population shrinkage.

Maintaining population diversity is the first step. Population reduction may lead to the removal of certain individuals, thus reducing the diversity of the population. The diversity of the population can be maintained through removal, making it more likely that the algorithm will find a globally optimal solution.

The complexity of the algorithm should be reduced. The population reduction operation increases the complexity of the algorithm, requiring additional parameters and calculations. Removing the population reduction simplifies the implementation and understanding of the algorithm, making it less difficult to implement.

It is necessary to avoid premature convergence. The population reduction may cause the algorithm to converge to a local optimum solution too early, thus failing to discover a better solution. Deleting this operation avoids premature convergence and allows the algorithm more opportunities to explore in the search space.

Last but not least, increasing the robustness of the algorithm is an important task. The population reduction may make the algorithm more sensitive to initial and tuning parameters. Removing this operation increases the robustness of the algorithm, making the algorithm more insensitive to the choice of parameters.

Overall, removing the population reduction operation can make the algorithm simpler, more varied and more robust, which will help to improve the performance and effectiveness of the algorithm.

(2) Improvement of the first defence stage.

Some randomness and variability are introduced for a better exploration of the search space, and the improved expression is shown below:

$$\vec{x_i^{t+1}} = \vec{x_i^t} + \left| \vec{x_{CP}^t} - \vec{x_i^t} \right| \times \theta \tag{32}$$

where $\vec{x_{CP}^t}$ is the best solution of the evaluation function t and θ is a random value in the interval [0, 1].

(3) The improved expression for the second defence phase is as follows:

$$\vec{x_i^{t+1}} = \left(1 - \vec{U_1}\right) \times \vec{x_i^t} + \vec{U_1} \times \left(\vec{y} + \theta\left(\vec{x_{r_1}^t} - \vec{x_{r_2}^t}\right)\right) \tag{33}$$

$$\vec{y_i^t} = \frac{\vec{x_i^t} - \vec{x_{r_3}^t}}{2} \tag{34}$$

where r_1, r_2 and r_3 are two random integers between [1, N].

(4) Improvements to the fourth defence stage.

It is necessary to reduce dependence on individual fitness. In the original equation, Mi relies on individual fitness to calculate the probability distribution; the improvement

directly uses random individuals in the population, reducing the calculation and the dependence on fitness.

It is important to improved algorithmic diversity and exploration. The new form introduces more randomness, which increases the diversity of the algorithm through the random number θ. The use of random numbers adjusts the position of individuals, which helps to explore the search space more extensively.

Dependence on a global optimal solution should be reduced. The improved catch uses individuals from the population, reducing the dependence on global information and making the algorithm more independent and flexible.

The improved expression for the fourth defence stage is shown as follows:

$$\vec{x_i^{t+1}} = \vec{x_{CP}^t} + (\theta(1-\tau_2)+\tau_2) \times \left(\vec{x_{CP}^t} - \vec{x_i^t}\right) \tag{35}$$

where $\vec{x_{CP}^t}$ is the best solution obtained, which denotes the position of the i-th individual at iteration t of $\vec{x_i^t}$ and denotes the predator at that position, and τ_2 is a random value in the interval [0, 1].

4.2. Application Analysis of the ICPO-LSTM Model

In order to verify the optimisation effect of the improved ICPO on the LSTM model, the ICPO-LSTM soft rock tunnel deformation prediction model is constructed. In this experiment, the ZK6 + 824 and ZK6 + 829 sections are used as the research object, and for the vault settlement and the upper conductor convergence curves of the ZK6 + 824 and ZK6 + 829 sections, see Figure 8a,b, respectively.

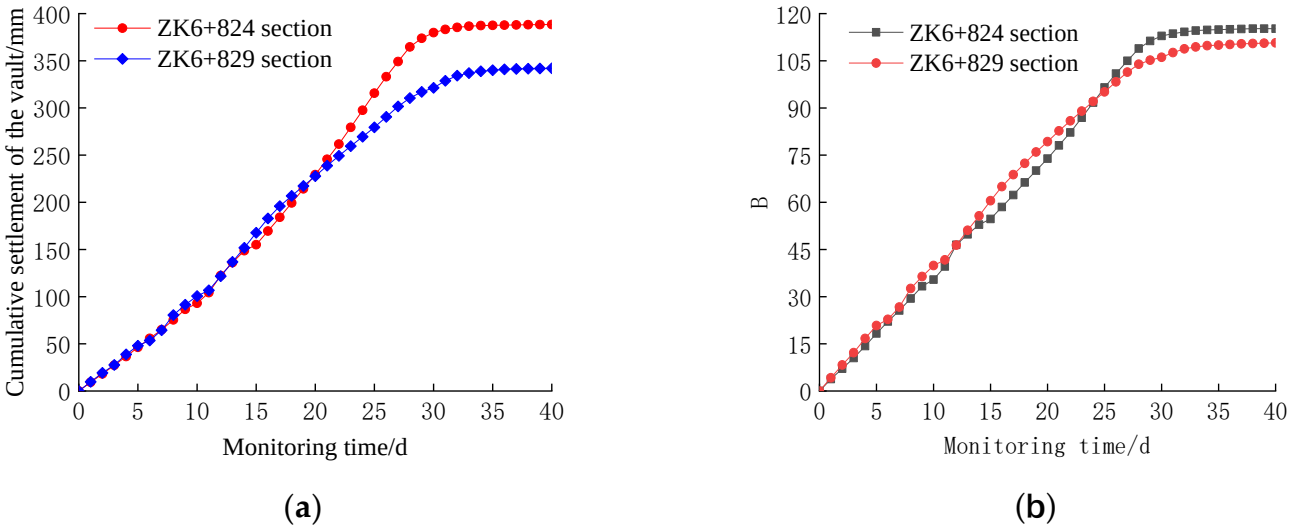

Figure 8. (**a**) ZK6 + 824, ZK6 + 829 section vault settlement monitoring curves map; (**b**) ZK6 + 824, ZK6 + 829 section of the upper conductor convergence monitoring curves map.

The data are divided into training and prediction sets; the top 70% of the data set is taken as the training set, and the bottom 30% is taken as the prediction set; the population number is 25, and the maximum number of iterations is 50. For the fitness evolution curves of the ICPO and CPO optimisation algorithms, see Figure 9a,b, respectively.

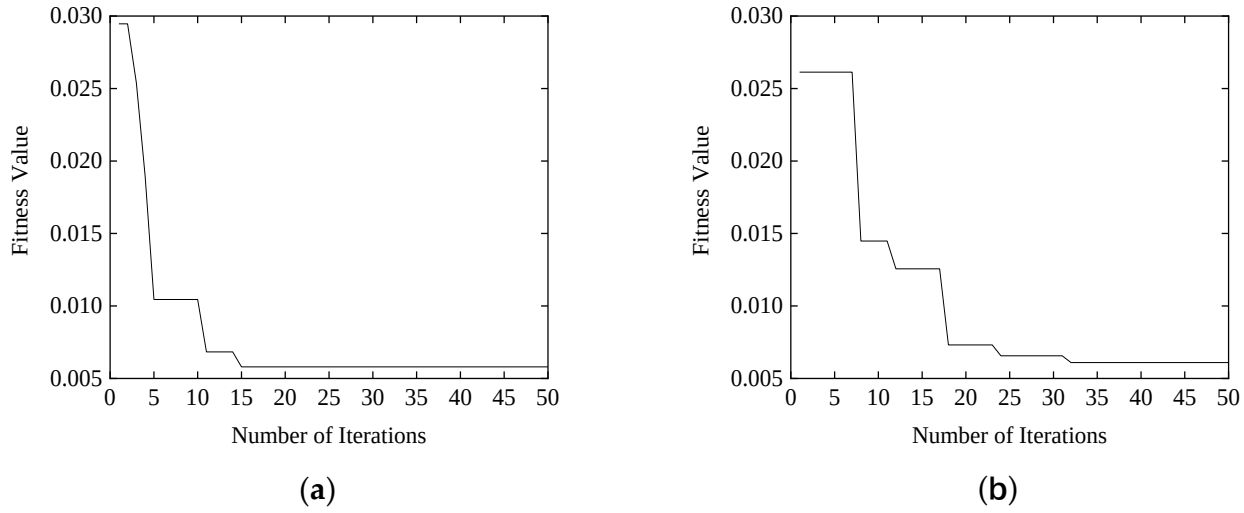

Figure 9. (**a**) ICPO fitness curve; (**b**) CPO fitness curve.

From Figure 9a,b, it can be seen that with the same initial parameters, the ICPO starts to converge at the 15th iteration with a fitness of 0.0058 and the CPO starts to converge at the 32th iteration with a fitness of 0.0061. It is obvious that the ICPO can find the globally optimal solution faster and its convergence error is smaller than the CPO, which indicates that the ICPO has a faster convergence speed and better computational results. It can be proved that the ICPO can successfully find the global optimal solution.

Figures 10 and 11 show the comparison of the prediction of vault settlement by different models and the prediction of the upper conductor by different models, respectively. From Figures 10 and 11 it can be seen that, in general, the improved ICPO-LSTM model predicts better than the CPO-LSTM model and the prediction accuracy is improved.

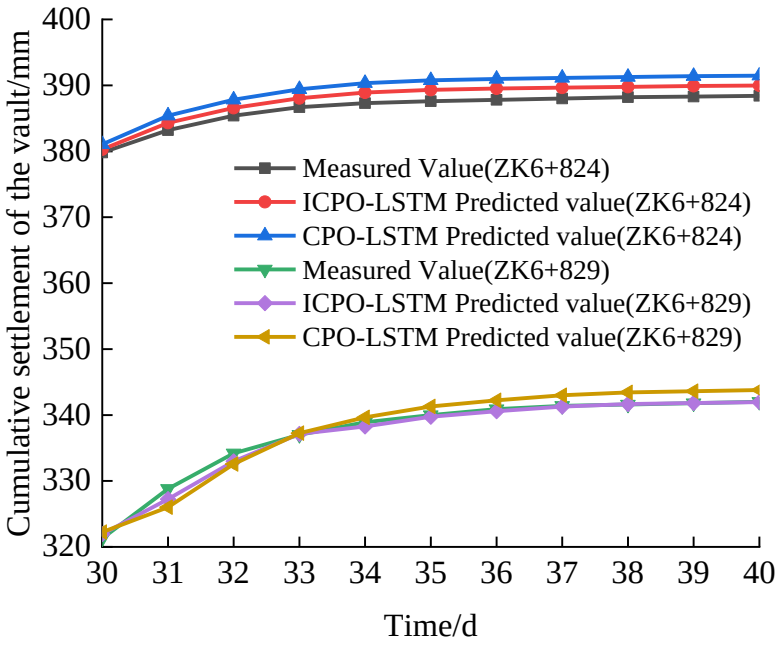

Figure 10. Comparison of the vault settlement predictions from different models.

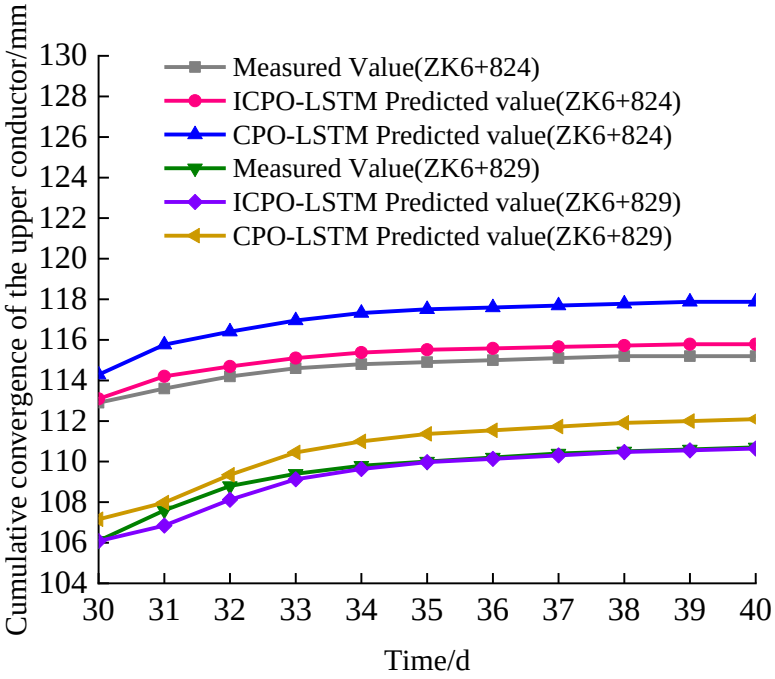

Figure 11. Comparison of the upper conductor predictions from different models.

As shown in Table 3, the average values of R^2, $MAPE$ and $RMSE$ of the ICPO-LSTM model are 0.9999, 0.2970 and 0.6273, respectively, while the average values of the corresponding metrics of the CPO-LSTM model are 0.9990, 0.9795 and 1.6639. It can be seen that the R^2 metrics of the ICPO-LSTM model are closer to 1, the fitting effect is better and it can better capture the potential patterns of the time series data. The $MAPE$ and $RMSE$ of the ICPO-LSTM model are significantly lower than those of the CPO-LSTM model, and the prediction accuracy is significantly improved. This further demonstrates that the optimisation capability of the improved CPO is further enhanced.

Table 3. Model evaluation index.

Predictive Model	Evaluation Indicators	ZK6 + 824 Section		ZK6 + 829 Section		Average Value
		Vault Monitoring Point	Upper Conductor Monitoring Point	Vault Monitoring Point	Upper Guide Monitoring Point	
ICPO-LSTM	R^2	0.9999	0.9998	0.9999	0.9999	0.9999
	$MAPE$/%	0.2447	0.4607	0.2977	0.1847	0.2970
	$RMSE$	0.9743	0.5404	0.6703	0.3240	0.6273
CPO-LSTM	R^2	0.9999	0.9969	0.9999	0.9991	0.9990
	$MAPE$/%	0.3659	2.0879	0.4324	1.0320	0.9795
	$RMSE$	1.4600	2.4221	1.5909	1.1825	1.6639

5. Discussion

Soft rock tunnels are easily affected by surrounding rock deformation and instability factors during construction, which can lead to tunnel collapse, cracking, deformation and other problems, bringing risks and difficulties to construction. By intelligently predicting the surrounding rock deformation, it can provide a guidance basis, reduce the construction risk and improve the safety and economic benefits of the project. Therefore, an intelligent prediction model based on CPO-LSTM is proposed. In order to verify the predictive effect of the established model algorithm on the measured tunnel vault settlement and upper guide-level convergence data, comparative analyses are carried out with the LSTM, CPO-GRNN and WOA-LSTM models, and it can be seen in Figures 6 and 7 that the prediction curves of the CPO-LSTM model are highly consistent with the actual curves, indicating

that the model performs better in terms of predictive performance. According to the information in Table 2, the goodness of fit of the CPO-LSTM model is 0.9997, the mean absolute percentage error is 0.3727% and the root mean square error is 0.1700, while the goodness of fit of the LSTM model is 0.9991, the mean absolute percentage error is 0.8956% and the root mean square error is 1.9358. The goodness of fit of the CPO-GRNN model is 0.9952, the mean absolute percentage error is 1.8574% and the root mean square error is 3.5077, while the WOA-LSTM model has a goodness of fit of 0.9967, the mean absolute percentage error is 1.7439% and the root mean square error is 3.2282. The three evaluation indices of the CPO-LSTM model are optimal, which shows that the prediction performance of the CPO-LSTM model is better than the LSTM, CPO-GRNN and WOA-LSTM models.

In order to investigate whether the performance of the CPO can be further improved, some improvements are made to the CPO and an Improved Crested Porcupine Optimiser (ICPO) is proposed. The ICPO-LSTM prediction model is built and compared with the original CPO-LSTM model, to verify whether the optimisation performance of the improved ICPO is improved. Figure 9 shows that the ICPO algorithm starts to converge at the 15th iteration, while the CPO algorithm starts to converge at the 32nd iteration. This indicates that the ICPO algorithm converges faster and is able to find the optimal solution in fewer iterations. The fitness value of the ICPO algorithm at the time of convergence is 0.0058, while that of the CPO algorithm at the time of convergence is 0.0061; because the lower fitness value indicates a closer optimal solution to the optimal solution, the solution obtained by the ICPO algorithm at the time of convergence is better than that of the CPO algorithm. From Figures 10 and 11 and Table 3, it can be seen that the maximum error of the ICPO-LSTM model is 2.161 mm, the minimum error is 0.012 mm, the goodness of fit is 0.9999, the average absolute percentage error is 0.2970% and the root mean square error is 0.6273, and the maximum error of the CPO-LSTM model is 3.565 mm, the minimum error is 0.378 mm, and the goodness of fit is 0.378 mm. The prediction accuracy of the ICPO-LSTM model is significantly better than that of the CPO-LSTM model. Numerical experimental studies have shown that the optimisation capability of the improved CPO has been enhanced.

6. Conclusions

(1) The average values of R^2, $MAPE$ and $RMSE$ of the CPO-LSTM model at ZK6 + 834 section are 0.9999, 0.3727% and 0.1700, respectively, which are better evaluation indices compared with the LSTM model, indicating that the optimisation of the LSTM model by the CPO algorithm can significantly improve the prediction accuracy of the model.

(2) The R^2, $MAPE$ and $RMSE$ metrics of the CPO-RGNN and WOA-LSTM models are worse than those of the CPO-LSTM model, indicating that the LSTM model optimised by the new optimisation algorithm performs better than the traditional machine learning and optimisation algorithms.

(3) The prediction accuracy of the improved ICPO-LSTM model is further improved compared to that of the CPO-LSTM model, and the three evaluation metrics of the ICPO-LSTM model, namely, R^2, $MAPE$ and $RMSE$, are all optimal. It is verified that the performance of the improved ICPO is improved compared with that of the CPO, and the ICPO-LSTM prediction model is able to provide a certain guidance basis for tunnel construction.

Author Contributions: Conceptualisation, C.Z. and H.L.; methodology, C.Z.; software, C.Z.; validation, J.C., H.L. and C.Z.; formal analysis, Y.P.; investigation, Y.P.; resources, W.D.; data curation, H.L.; writing—original draft preparation, C.Z.; writing—review and editing, H.L.; visualisation, W.D.; supervision, H.L.; project administration, J.C.; funding acquisition, H.L. All authors have read and agreed to the published version of the manuscript.

Funding: The preparation of the paper received financial support from the Scientific Research Fund of the Institute of Engineering Mechanics, China Earthquake Administration (Grant No. 2020EEEVL0204) and the Yunnan Province Major Science and Technology Special Plan Project (202102AF080001-2). The financial support is greatly appreciated.

Data Availability Statement: For privacy reasons, the data cannot be made fully public. Readers can contact the corresponding author for details.

Conflicts of Interest: Author Wenyun Ding was employed by the company Kunming Survey, Design and Research Institute Co., Ltd. of CREEC. The remaining authors declare that the research was conducted in the absence of any commercial or financial relationships that could be construed as a potential conflict of interest.

References

1. Yang, J.S.; Xia, Y.D.; Fang, X.H.; Liu, W.L.; Wang, F.L. Research on large deformation and control technology of tunnel surrounding rock in jointed carbonaceous shale strata. *J. Cent. South Univ. (Nat. Sci. Ed.)* **2024**, *55*, 188–200.
2. Guo, X.X.; Wang, B.; Wang, Z.Y.; Yu, J.W. Methods and practices of deformation prediction in high-stress soft rock tunnels considering creep characteristics. *J. Geotech. Eng.* **2023**, *45*, 652–660.
3. Song, G.; Zhou, P.; Hu, Q. Application of Improved Grey Model Based on Cumulative Method to Deformation Prediction of Tunnel Surrounding Rock. *J. Phys. Conf. Ser. IOP Publ.* **2020**, *1676*, 012241. [CrossRef]
4. Xiong, X. Research on grey system model and its application on displacement prediction in tunnel surrounding rock. *Open Mech. Eng. J.* **2014**, *8*, 514–518. [CrossRef]
5. Qiang, Y.; Li, S.H.; Liu, C.Q. Prediction and application of tunnel surrounding rock deformation based on multi-scale combined kernel limit learning machine model. *Mod. Tunneling Technol.* **2017**, *54*, 70–76.
6. Zhao, S.M. Research on the application of quantization theory III and limit learning machine based on quantization theory III and limit learning machine in the analysis of deformation influencing factors of small clear distance tunnel. *Tunn. Constr.* **2018**, *38*, 1456–1462, (In Chinese and English)
7. Zhou, Q.C.; Fan, S.Y.; Zhao, J.; Xiong, X.L. Tunnel deformation prediction model based on improved support vector machine. *J. Railw. Eng.* **2015**, *32*, 67–72.
8. Lv, Q.F.; Li, Y.; Niu, R.; Xu, X.H.; Mao, N.; Kang, Q.Y. Deep learning-based prediction of surrounding rock deformation in special geotechnical tunnels. *J. Appl. Basic Eng. Sci.* **2023**, *31*, 1590–1600.
9. Wang, S.H.; Dong, F.R. Stability analysis of surrounding rock in mountain tunnels based on deformation prediction and parameter inversion. *J. Geotech. Eng.* **2023**, *45*, 1024–1035.
10. Zhang, Z.; Pan, Q.; Yang, Z.; Yang, X.L. Physics-informed deep learning method for predicting tunnelling-induced ground deformations. *Acta Geotech.* **2023**, *18*, 4957–4972. [CrossRef]
11. Li, Z.Z.; Wang, H.; Chang, X.Y.; Zhang, Y.M.; Wang, F.Q. Convergence and deformation prediction of high speed rail tunnel surrounding rock based on combined model. *J. Southeast Univ. (Nat. Sci. Ed.)* **2021**, *51*, 851–858.
12. Yue, L.; Liu, F.; Liu, H.; Cao, L.Q. Prediction and analysis of ground deformation in large diameter shield tunnel construction based on artificial neural network. *Railw. Stand. Des.* **2020**, *64*, 122–126.
13. He, Y.; Chen, Q. Construction and Application of LSTM-Based Prediction Model for Tunnel Surrounding Rock Deformation. *Sustainability* **2023**, *15*, 6877. [CrossRef]
14. Yu, T.; Pei, L.L.; Li, W.; Hu, Y.J.; Yang, M. Prediction of Pavement Surface Condition Index Based on Random Forest Algorithm. *Highw. Traffic Sci. Technol.* **2021**, *38*, 16–23. [CrossRef]
15. Li, W.W.; Li, X.Y.; Zhou, J.; Xie, Y.H.; Li, G. An Algorithm for Recognizing Bridge Cracks Based on Full Convolution Neural Network and Naive Bayesian Data Fusion. *Highw. Traffic Sci. Technol.* **2023**, *40*, 44–52.
16. Zhou, G.N.; Sun, Y.Y.; Jia, P. Application of BP neural network based on genetic algorithm in inversion of tunnel surrounding rock parameters and deformation prediction. *Mod. Tunneling Technol.* **2018**, *55*, 107–113.
17. Huang, Z.; Liao, M.; Zhang, H.; Zhang, J.; Ma, S.; Zhu, Q. Predicting tunnel squeezing using the SVM-BP combination model. *Geotech. Geol. Eng.* **2022**, *40*, 1387–1405. [CrossRef]
18. Xue, Y.; Ma, X.; Qiu, D.; Yang, W.; Li, X.; Kong, F.; Zhou, B.; Qu, C. Analysis of the factors influencing the nonuniform deformation and a deformation prediction model of soft rock tunnels by data mining. *Tunn. Undergr. Space Technol.* **2021**, *109*, 103769. [CrossRef]
19. Wu, H.; Chen, Y.T.; Zhu, Z.H.; Li, X.W.; Yu, Q. Improved one-dimensional convolutional neural network for hierarchical prediction of convergent deformation of tunnel surrounding rock. *J. Appl. Basic Eng. Sci.* **2024**, *32*, 145–159.
20. Wu, C.; Hong, L.; Wang, L.; Zhang, R.; Pijush, S.; Zhang, W. Prediction of wall deflection induced by braced excavation in spatially variable soils via convolutional neural network. *Gondwana Res.* **2023**, *123*, 184–197. [CrossRef]
21. Zhang, K.; Lyu, H.M.; Shen, S.L.; Zhou, A.; Yin, Z.-Y. Evolutionary hybrid neural network approach to predict shield tunneling-induced ground settlements. *Tunn. Undergr. Space Technol.* **2020**, *106*, 103594. [CrossRef]
22. Freitag, S.; Cao, B.T.; Ninić, J.; Meschke, G. Recurrent neural networks and proper orthogonal decomposition with interval data for real-time predictions of mechanised tunnelling processes. *Comput. Struct.* **2018**, *207*, 258–273. [CrossRef]

23. Cao, Y.; Zhou, X.; Yan, K. Deep learning neural network model for tunnel ground surface settlement prediction based on sensor data. *Math. Probl. Eng.* **2021**, *2021*, 9488892. [CrossRef]
24. Ma, K.; Chen, L.P.; Fang, Q.; Hong, X.-F. Machine learning in conventional tunnel deformation in high in situ stress regions. *Symmetry* **2022**, *14*, 513. [CrossRef]
25. Yao, K.; Zhu, X.Y.; Zhang, K.H.; Zhang, X.X.; Wang, K.L. Prediction model of surrounding rock deformation in soft rock tunnels based on FOA-GRNN. *J. Undergr. Space Eng.* **2019**, *15*, 908–913.
26. Pan, Y.; Chen, L.; Wang, J.; Ma, H.; Cai, S.; Pu, S.; Duan, J.; Gao, L.; Li, E. Research on deformation prediction of tunnel surrounding rock using the model combining firefly algorithm and nonlinear auto-regressive dynamic neural network. *Eng. Comput.* **2021**, *37*, 1443–1453. [CrossRef]
27. Huang, Z.; Liao, M.X.; Zhang, H.L.; Zhang, J.B.; Ma, S.K. Prediction of extrusion deformation of tunnel surrounding rock based on non-complete data of SVM-BP model. *Mod. Tunneling Technol.* **2020**, *57*, 129–138.
28. Xu, W.; Cheng, M.; Xu, X.; Chen, C.; Liu, W. Deep learning method on deformation prediction for large-section tunnels. *Symmetry* **2022**, *14*, 2019. [CrossRef]
29. Ye, X.W.; Zhang, X.L.; Zhang, H.Q.; Ding, Y.; Chen, Y.-M. Prediction of lining upward movement during shield tunneling using machine learning algorithms and field monitoring data. *Transp. Geotech.* **2023**, *41*, 101002. [CrossRef]
30. Kang, Q.; Chen, E.J.; Li, Z.C.; Luo, H.-B.; Liu, Y. Attention-based LSTM predictive model for the attitude and position of shield machine in tunneling. *Undergr. Space* **2023**, *13*, 335–350. [CrossRef]
31. He, R.G.; Zhang, X.Y.; Wang, X.; Wang, X.; Zhao, Z.Y.; An, S.B. A deep learning-based method for analyzing and predicting metro tunnel monitoring and measurement data. *Tunn. Constr.* **2021**, *41*, 261–267, (In Chinese and English)
32. Abdel-Basset, M.; Mohamed, R.; Abouhawwash, M. Crested Porcupine Optimizer: A new nature-inspired metaheuristic. *Knowl.-Based Syst.* **2024**, *284*, 111257. [CrossRef]
33. Specht, D.F. A General Regression Neural Network. *IEEE Trans. Neural Netw.* **1991**, *2*, 568–576. [CrossRef] [PubMed]
34. Mirjalili, S.; Lewis, A.D. The Whale Optimization Algorithm. *Adv. Eng. Softw.* **2016**, *95*, 51–67. [CrossRef]